ELSEVIER

Experimental Thermal and Fluid Science 18 (1998) 258–269

Experimental Thermal and Fluid Science

Experimental design for flowfield studies of louvered fins

Marlow E. Springer, Karen A. Thole *

Mechanical Engineering Department, University of Wisconsin, 1513 University Avenue, Madison, WI 537061572, USA

Received 10 September 1997; received in revised form 12 March 1998; accepted 22 April 1998

Abstract

The dominant thermal resistance for most compact heat exchangers occurs on the gas side and as such an understanding of the gas side flowfield is needed before improving current designs. Louvered fins are commonly used in many compact heat exchangers to increase the surface area and initiate new boundary layer growth. Detailed measurements can be accomplished with large-scale models of these louvered fins to gain a better understanding of the flowfield. This paper describes a methodology used for designing an experimental model of a two-dimensional louvered fin geometry, scaled up by a factor of 20, that allows for flowfield measurements. The particular louver geometry studied for these experiments had a louver angle of 27° and a ratio of fin pitch to louver pitch of 0.76. Simulations using computational fluid dynamics (CFD) both aided in designing the large-scale louver model, resulting in a total number of 19 louver rows, and identified the region where the flowfield could be considered as periodic. This paper also presents two component velocity measurements taken in the scaled up model at Reynolds numbers of $Re = 230$, 450, and 1016. For all three Reynolds numbers the flow was louver directed rather than duct directed. The results indicated that significant differences between the three Reynolds numbers occurred. While the flow entering the louver passage at $Re = 1016$ still had remnants of the louver wake convected from two louvers upstream, the $Re = 230$ case did not. Time-resolved velocity measurements were also made in the wake region of a fully developed louver for a range of Reynolds numbers. For $1000 < Re < 1900$, there was an identifiable peak frequency for the velocity fluctuations giving a constant Strouhal number of $St = 0.17$.

Keywords: Heat exchangers; Louvered fins; Interrupted surfaces

1. Introduction

Optimizing compact heat exchangers to both maximize heat transfer and minimize the pressure drop is of concern to vehicular, industrial, and building markets. Improving the efficiency and quality control of air-cooled heat exchangers is needed to ultimately reduce the space, weight, and cost requirements for compact heat exchangers. Because the dominant thermal resistance for most air-and-water or air-and-oil compact heat exchangers occurs on the air side, an understanding of the air flowfield dictating the heat transfer and pressure drop is needed to further optimize these heat exchangers.

Louvered fins, which are also referred to as interrupted surfaces, are commonly used in heat exchanger designs for reasons beyond simply increasing the convective heat transfer surface area. Provided that the gas side heat exchanger fluid, such as air, flows through the louvers as opposed to flowing axially, laminar boundary layers develop along the louvers. The louvers then break up the growth of this boundary layer resulting in high heat transfer rates in the initial re-growth regions. In addition to promoting the boundary layer re-growth, the louvers provide a means for vortex shedding from the trailing edge, which can impact the boundary layers on the neighboring louvers and be used as a mechanism to increase the local heat transfer rates.

One possible tool for optimizing the louver geometry is to use CFD models, which typically assume laminar, two-dimensional, steady flows with periodic boundary conditions. As the vortex shedding becomes increasingly important, however, the steady flow and laminar flow assumptions are questionable and it becomes even more important to benchmark CFD models with experimental data. To provide detailed experimental data in which periodic flow conditions can be assumed, care must be taken to design models that are scaled up to give good measurement resolution and to ensure that the relevant flowfield features are met.

* Corresponding author. Tel.: +1-608 262-0923; fax: +1-608 265-2316; e-mail: thole@engr.wisc.edu.

0894-1777/98/$19.00
PII: S0894-1777(98)10022-5

Table 1
Summary of scaled-up louvered fin geometry[a]

Louver angle (θ)	27°
Louver pitch (L_P)	27.9 mm
Fin pitch (F_P)	21.2 mm
Fin thickness (t)	2.3 mm
Number of louvers	17
Scale factor for testing	20

[a] Geometry and scaled-up model were supplied by Modine Manufacturing Company.

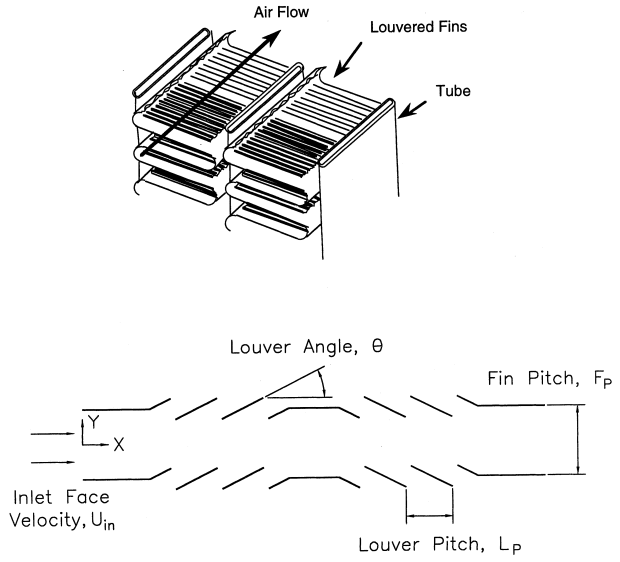

Fig. 1. (a) and (b) Illustration of the louvered plate fin heat exchanger and important parameters for the finned louver geometry.

The flowfield associated with the fin/louver combination is influenced by a number of geometrical parameters, as has been shown in previously reported studies. Geometrical parameters including the fin pitch (F_P) relative to the louver pitch (L_P), the number of louvers, and the angle (θ), length (l), and thickness (t) of the louvers all affect the heat transfer characteristics. The questions that still remain are twofold. First, under what conditions does the gas-side fluid follow the louvers as opposed to being directed axially? Second, is it possible to detect any time periodicity to the flow at the trailing edge of the louvers and, if so, is it a function of Reynolds number?

The purpose of this paper is to present a methodology of determining an experimental design for testing a scaled-up louver/fin arrangement. The specific geometry for this study is listed in Table 1. To ensure that the measured flow was periodic and not influenced by endwall effects, the question became how many rows of louvers were needed for the experiments. After the scaled-up model was designed through the use of CFD, the periodicity was experimentally verified in regions of the large-scale model where the CFD predicted the flow to be periodic. This paper also presents detailed flowfield measurements for this louver geometry, made using a non-intrusive laser Doppler velocimeter (LDV) at three different Reynolds numbers of Re = 230, 450, and 1016, where Reynolds numbers are based on the louver pitch and the inlet face velocity. In addition, the energy spectra of the measured velocity fluctuations downstream of the louver trailing edge were quantified.

2. Previous studies

Detailed louvered fin studies date back to the flow visualization studies performed by Beauvais [1] in 1965. Since that time, there have been reported flow visualization studies, flow measurements primarily using intrusive techniques, and CFD studies. The studies discussed in this section have focused on a louvered fin-and-tube design illustrated in Fig. 1(a) whereby the focus is on the louvered fin design with the geometrical parameters of interest illustrated in Fig. 1(b).

Heat transfer and pressure drop performance studies by Achaichia and Cowell [2] confirmed the theory by Davenport [3] who suggested that two types of flow conditions existed depending on Reynolds number based on louver pitch. Davenport reasoned that at low Reynolds numbers, the louver boundary layers were so thick that flow between the louver gaps was essentially blocked such that the flow became axially directed or also known as duct directed. Achaichia and Cowell in fact found the flow to travel axially for a $Re < 40$. The numerical heat transfer predictions of Achaichia and Cowell showed that at these low Reynolds numbers, the average heat transfer coefficients approached that of duct type flows.

At the intermediate Reynolds numbers there is still some disagreement as to when the flow is louver or duct directed as illustrated when comparing the numerical predictions presented by Achaichia and Cowell [2] to those estimated through flow visualization studies conducted by Webb and Trauger [4]. For a louver angle of $\theta = 30°$ and a ratio of the fin pitch to louver pitch of $F_P/L_P = 1.50$, Webb and Trauger [4] indicate that as the Reynolds number decreases below 1000 the flow efficiency begins to rapidly decrease while the predictions of Achaichia and Cowell [2] do not show a rapid decrease in the ratio of the flow angle to louver angle until the Reynolds number decreases below 100. Note that the flow efficiency, defined by Webb and Trauger as the ratio of the actual flow path to the ideal flow path, is much like the ratio of the flow angle to louver angle.

Data in the literature do not indicate a consistency at the intermediate Reynolds numbers as to whether the flow is duct or louver directed. In part, the reason for this lack of consistency may be due to the experimental set-up itself. The experimental test sections reported in the literature can have a much different boundary condition than the CFD studies in which periodic boundary conditions are assumed. Experiments are typically set up by having, for example, a number of louver rows where

this number can vary anywhere between five and ten rows. Maintaining enough rows of louvers should allow for direct comparisons between measurements and computations with periodic boundary conditions. As fewer and fewer rows of louvers are used, the flow is forced to become duct directed because of the endwall effects, as will be discussed in the later sections.

CFD studies done by Suga and Aoki [5] have attempted to optimize the performance of the louver geometry from a heat transfer and pressure drop performance. Suga and Aoki proposed a geometrical relation for predicting the optimum ratio of the fin pitch to louver pitch whereby they predicted the optimum to occur when a line can be extended from the trailing edge of the louver to reach the mid point between the next pair of downstream louvers. The geometry used in this flowfield study was predicted by Suga and Aoki's correlation as being an optimal geometry for this louver angle.

Two distinct flowfield mechanisms, depending upon the conditions, can appear as increased velocity fluctuations in this primarily laminar flow. For a louver directed flow, as the louver angle is increased the flow can separate from the louver causing increased fluctuations. This separated flow is distinctly different from the laminar flow that remains attached to the louvers which produce a wake region downstream of the louver plate. Although the vortex shedding phenomenon has not been characterized experimentally for inclined louvers, detailed flowfield measurements by Antoniou et al. [6] did show a significant increase in velocity fluctuations. Antoniou et al. used hot-wire anemometry to quantify the flowfield and reported high fluctuation levels at $Re = 1000$. Antoniou et al. hypothesized that these high fluctuations were vortices being shed from the louvers since their flow was primarily louver directed. Flow visualization results reported by DeJong and Jacobi [7] for a parallel array of staggered interrupted surfaces indicated that at $Re = 380$ there was a steady recirculating eddy behind the fin and at $Re = 850$ there were shedding vortices. This has also been observed in the time-dependent computations of flows over in-line and staggered interrupted surfaces by Zhang et al. [8].

Clearly, the past studies point to a need for more detailed flowfield measurements that quantify mean and time-resolved velocities. To compare with CFD studies using periodic boundary conditions, it is important to benchmark those computations with experimental data obtained in the same manner. Because these flows are either laminar/steady at low Reynolds numbers or laminar/unsteady or transitional at intermediate Reynolds numbers, it is desirable to quantify this flowfield with a non-obtrusive technique so as not to disturb flow.

3. Design of large-scale louvered fin model

This study used a combined CFD and experimental approach where CFD was used to design the experimental test rig and identify regions were the flowfield could be considered to be periodic. The computations were performed using a code that solved the Navier–Stokes equations with a pressure-based, finite volume scheme. The SIMPLE algorithm, with second order accuracy, was used to solve the discretized equations with a multi-grid acceleration. This solver was included in the CFD package from FLUENT [9] which also included an unstructured triangular mesh generator. The flow for all of the computations presented in this paper was considered to be two-dimensional, steady, and laminar.

Several grid adaptions, based on computed flow gradients, resulted in a final mesh with 240 000 cells for the full-scale simulation of 19 louver rows. The average cell skewness for this mesh was 0.2 with a maximum skewness of 0.4. The convergence criterion used for each adaption was that residuals for u, v, and continuity dropped by three orders of magnitude, to at least 10^{-3} or smaller. The computations were done using 6 nodes of a 16 node IBM-SP2 and took approximately 4 h to complete 300 iterations, which was needed for one grid adaption.

The computational predictions for the full test rig were not meant to be quantitatively accurate but rather achieve a qualitative assessment as to the number of louver rows necessary to achieve flow periodicity over several louver passages. By examining the velocity magnitude profiles, a qualitative comparison between adjacent louver rows was used to determine the number of rows necessary to obtain periodic flow conditions. In addition, the CFD simulations also provided the locations where the flow was considered to be periodic and where the velocity measurements were to be made.

As 5–10 rows of louvers have been used in most of the past experimental studies, it was first thought that five rows would be enough to adequately simulate an actual heat exchanger. Note that a scale factor of 20 was chosen for the experimental model of the louvered fins to allow for good spatial resolution of the velocity measurements. The first step in the design was to run a CFD simulation of the five row model with end walls that were placed one-half fin pitch away from the end louver rows, to compare with the predictions using periodic boundary conditions.

Fig. 2(a)–(c) compare predictions of the flowfields at $Re = 230$ using periodic boundary conditions (Fig. 2(a)), using five louver rows with endwalls at one-half fin pitch away (Fig. 2(b)), and using 19 louver rows with the top end wall placed three fin pitches away (Fig. 2(c)). Fig. 2(a)–(c) show the fourth, fifth, and sixth streamwise louver positions. Note that Fig. 2(a) shows three vertical repeats of the periodic simulation. The vertical position shown for the five row simulation (Fig. 2(b)) is near the endwall with the top louver in the figure being in the vertical middle of the five rows. The vertical position shown for the 19 row simulation is in the region where the flow is considered periodic. These results clearly show that the flowfield for the five row simulation indicates duct directed flow, whereas the flowfield for both the periodic and 19 row simulations indicate louver di-

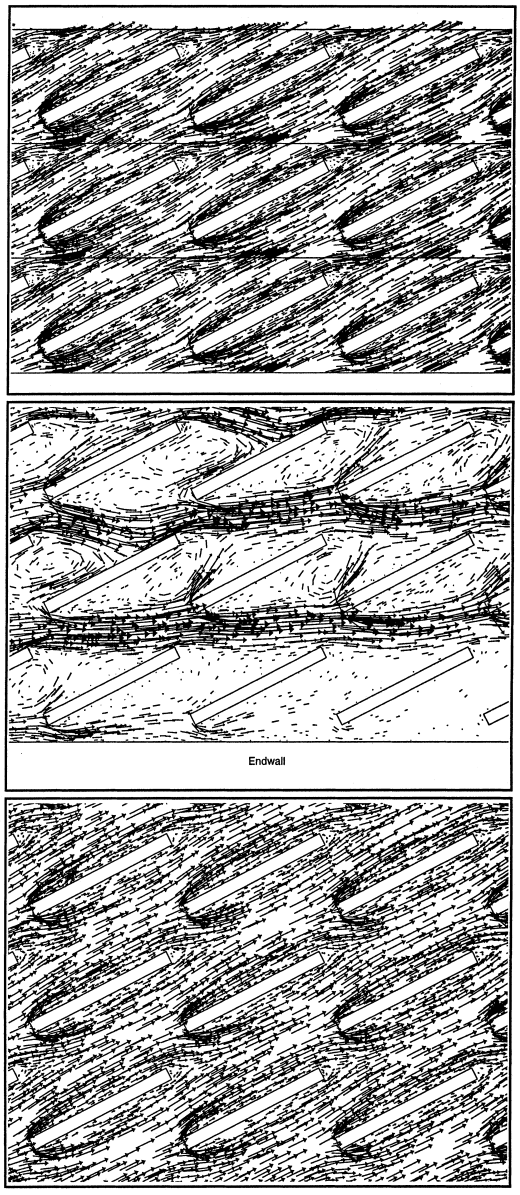

Fig. 2. CFD predictions showing differences in the flowfield for: (a) periodic boundary condition model; (b) 5 row model; and (c) 19 row model.

rected flow. It is evident that the endwalls have a significant effect on the flow as indicated by the five row simulations, making it impossible to achieve a periodic flow in the section. In order to remedy the problems seen in the results of the five row model, the number of louver rows was increased until the point was reached where there were at least four louver passages (bounded by five louvers) that exhibited the same mean flow.

The CFD results also showed an effect of the flow restriction caused by the upper row of louvers yielding a significant downturning of the inlet flow for the five row model. Even when the number of rows was increased to 10 rows, this downturning still existed. To ensure that the flow entered the test section uniformly, the location of the top wall was varied. The final position of the top wall was spaced $3F_P$ from the top row of louvers, while the bottom wall was left spaced at $0.5F_P$ from the bottom row. With a larger spacing between the top wall and the first louver row, there was no longer the downturning effect that was initially caused by the absence of a flow path for the fluid entering the top of the large-scale model. A larger spacing was not needed for the bottom wall because the flow entering the bottom of the model was immediately directed upward and, since the test rig was symmetric in the streamwise direction, there was enough distance to complete the downturn before exiting the test rig.

4. Experimental facility and instrumentation

The experiments were carried out in a closed-loop flow arrangement, as shown in Fig. 3, with the majority of the loop being 15.2 cm diameter PVC pipe. The test section was 17.5 cm in depth, 44.1 cm in height, and 69.6 cm long. The louvers were cold rolled steel 2.3 mm thick. The front plate of the section, through which the laser beams pass for velocity measurements, was made of Lexan. The velocity measurements were made approximately 25.4 mm into the depth of the test section from the side wall. Flowfield measurements were made across the depth of the test section to ensure that the measurements reported in this paper were not influenced by the sidewall boundary layer. Typical operating temperatures were maintained at 24°C ± 1°C.

A settling chamber was used ahead of the test section to condition the flow entering the test section. Screens were also in place at the inlet to the chamber to distribute the incoming flow throughout the chamber rather than going directly into the test section. Foam and screens at the inlet to the large-scale model aided in achieving flow uniformity and reduced turbulence intensity levels. For the mean velocity measurements, the flow was driven by a 12 W (1/64 HP) in-line axial fan running at 3500 rpm. A manual butterfly valve was used to control the flow rates to achieve the various inlet Reynolds numbers. After measuring the first time-resolved data and performing a spectral analysis on the data at the inlet to the test section, it was apparent that there was a frequency close to the fan frequency that was dominating the spectra. After several iterations of tests, the axial fan and butterfly valve were replaced with a 373 W (1/2 HP) centrifugal fan running at a maximum of 3450 rpm. The rotation frequency of the fan varied between 5 and 60 Hz for Reynolds numbers ranging between 100 and 1900. A 3-phase variable-frequency motor controller was used to vary the fan frequencies and control the flowrate. In using the centrifugal fan, there still seemed to be a frequency component in the time-resolved data at the test section inlet. To completely quiet the flow, the settling chamber was filled with Styrofoam packaging 'popcorn', which prohibited any dominating system frequencies from entering the large-scale model. This left essentially no peaks in the

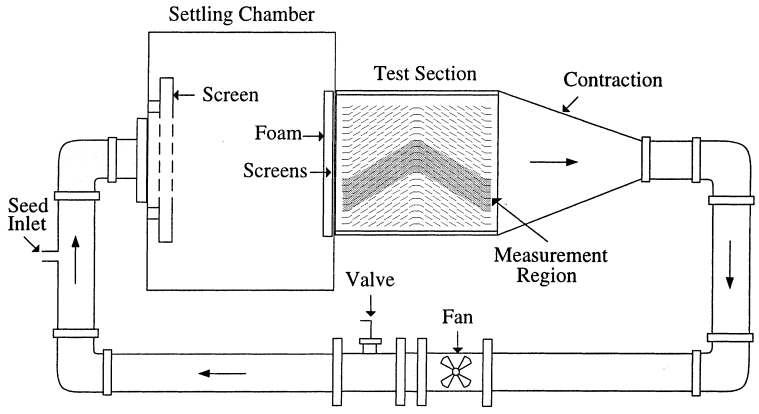

Fig. 3. Flow loop for velocity measurements in the large-scale model.

spectra at the inlet, and enabled the study of flow unsteadiness from the trailing edge of the louvers.

A two-component laser Doppler velocimetry (LDV) system was used to measure the mean and time-resolved velocities in the louvered fin array. A 5 W argon–ion laser with a backscatter fiber optic probe and digital burst correlator were used. The focal length of the lens was 350 mm, with a probe volume that is 90 μm in diameter and 1.3 mm in length. The movement of the probe was obtained with a two-component, computer-controlled traverse that moves to a position that is accurate to ±5 μm. The position relative to the louver location was determined by crossing the probe volume on the wall and was estimated for these studies to be within ±0.2 mm, or rather ±1% of the fin pitch. Incense smoke was generated outside the main loop and injected just upstream of the settling chamber as the LDV seed particles with nominal diameters of 1 μm.

Horizontal and vertical velocity components were measured whereby the mean velocities were obtained with 5000 points over a period of 20 s at each measurement location. For the time-resolved velocity measurements 30 000 points were obtained at a nominal data rate of 1000 samples per second for a sample time of 30 s. The mean velocities were calculated using residence time weighting as the velocity bias correction technique.

Time-resolved velocity measurements were also taken using the LDV data, as will be described later in the paper. This data was used to calculate the energy spectral densities by using a Fast Fourier Transform (FFT) routine in National Instruments' LABVIEW software. Typically, LDV data rates of 1000 samples per second were achieved while the frequencies of interest were below 100 Hz. The total number of data points for the FFT program ranged between 11 000 and 12 000 points. Approximately 45 averages were used for computing the spectra.

Velocity uncertainties were based on the method described by Moffat [10]. The bias uncertainty in the velocity measurements is estimated as 1%, arising from uncertainties in the Doppler frequencies and the fringe spacing. The velocity precision error with a 95% confidence interval is a maximum of 0.1% based on the mean velocity measurements for cases with and without vortex shedding. These lead to uncertainties in the measured velocity angle of about 1.7%.

5. Mean flowfield results

A number of different louver positions were measured as indicated in Fig. 4 where these cuts will be referred to by the louver number appearing above the louvers. Multiple profiles were measured in several louver passages (1a–c, 5a–e, 9a–c, and 13a–e) while single profiles were measured at the streamwise middle position of the louver passage at the other louver locations. The measurements were made orthogonal to the axial flow direction, and the normalized vertical coordinate that will be used, Y/H, is measured from the vertical center of the louver passage as indicated in Fig. 4. Throughout this section, the different sides of the louver will be referred to as the upstream side and the downstream side while the leading edge and trailing edge positions are along the louver as shown in Fig. 4. The flowfields were mapped for three different Reynolds numbers of $Re = 230$, 450, and 1016 where this Reynolds number is based on the louver pitch and the inlet face velocity.

Before starting to measure the flowfield, the periodicity of the flow was evaluated. As stated earlier, the CFD studies identified the region over which the flow could be considered periodic and the experimental measurements could be acquired. This region was indicated by the gray shading in Fig. 3. Since the flow is louver directed for this geometry, the measurement region follows a pathline through the test rig. Fig. 5 shows mean velocity magnitudes at $Re = 1016$ over three vertical louver positions in the fifth streamwise louver passage. The vertical position of the bottom profile in Fig. 5 is in the sixth passage from the bottom of the large scale model. The results indicate periodic flow conditions in the measurement region were achieved.

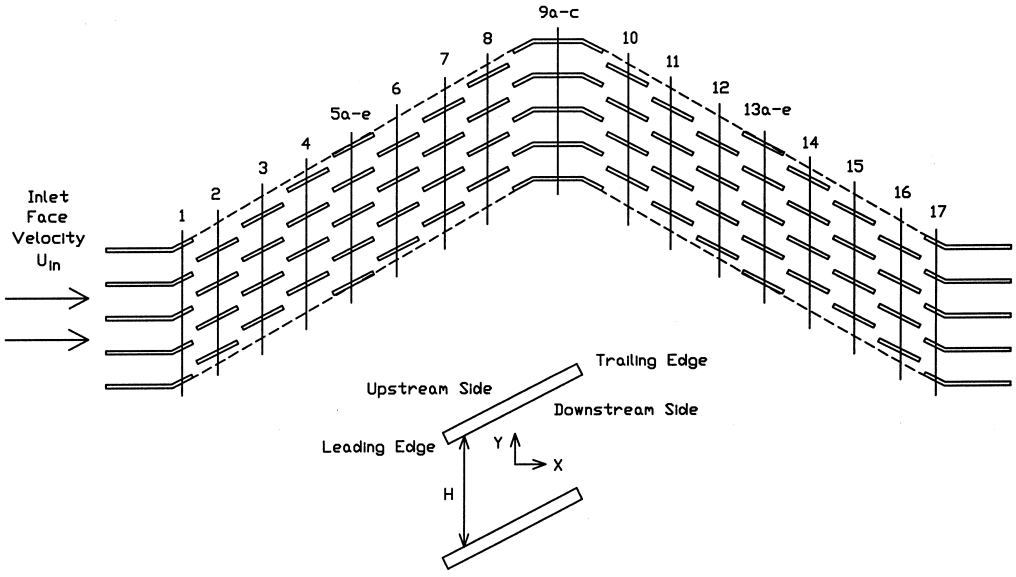

Fig. 4. Detail of measurement region showing cut locations of velocity profile measurements and louver terminology.

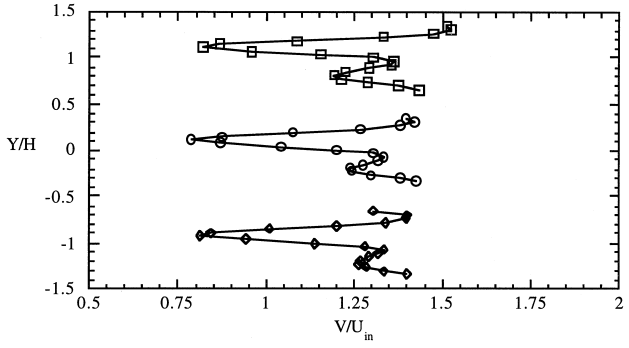

Fig. 5. Measured mean velocity magnitudes in three adjacent louver passages at Re = 1016.

To address the question as to whether the flow is louver or duct directed, the flow angles were calculated using the two measured velocity components. Fig. 6 presents the ratio of the average flow angle to louver angle ($\bar{\alpha}/\theta$) in comparison with predictions made by Achaichia and Cowell [2] and measurements made by Webb and Trauger [4], who both had louver geometries similar to the present study. The average flow angles shown in Fig. 6 are those averaged over a vertical distance of $0.75H$ in the fifth louver passage. For all three Reynolds numbers the flow is louver directed, which is in agreement with the past studies. Note that the correlation given by Achaichia and Cowell is slightly below both experimental data sets.

Fig. 7 shows the ratios of the flow angle to louver angle progressing streamwise along the louvers for Re = 230 and 1016. The flow is still adjusting at the first louver, as indicated by a $\bar{\alpha}/\theta$ ratio much less than one, but by the time the flow reaches the second louver the ratio is near one for both Reynolds numbers. The $\bar{\alpha}/\theta$ ratio for the Re = 230 case is slightly below that for the Re = 1016 case and, as the flow progresses downstream

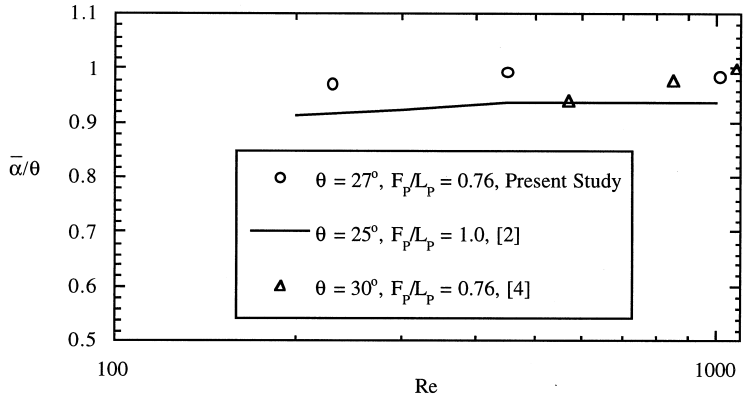

Fig. 6. Measured ratios of average flow angle to louver angles as a function of Reynolds number in the fifth louver passage compared with prediction by Achaichia and Cowell [2] and measurements by Webb and Trauger [4].

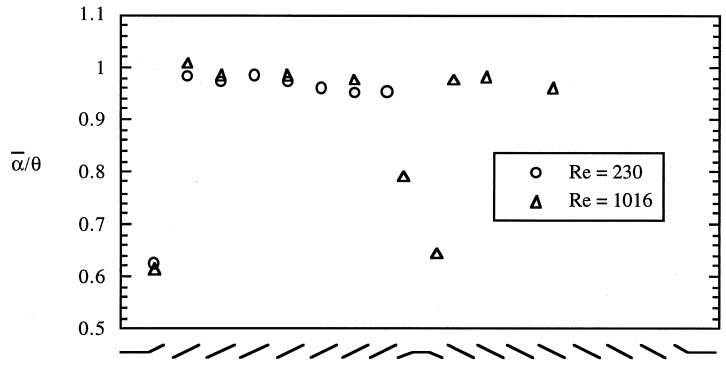

Fig. 7. Streamwise progression of measured average ratios of flow angle to louver angle at two Reynolds numbers.

towards the flow reversal louver, there is a slight decrease in the $\bar{\alpha}/\theta$ ratio. This decrease is a result of the boundary layers along the louvers becoming slightly thicker which is deflecting the flow away from the louver. In all cases the flow angle for the Re = 1016 case is higher than that of the Re = 230 case due to the thinner boundary layers at the higher Reynolds number. As the flow reversal occurs at louver 9, the flow angle decreases significantly but quickly returns to the louver direction by louver 10.

Fig. 8(a) and (b) give the total velocity profiles, normalized by the inlet face velocity, and the variation of the α/θ ratio throughout the louver passages upstream of the flow reversal louver for the Re = 230 case. The total velocity profiles are self-similar downstream of the second louver. Slightly above the middle of the louver

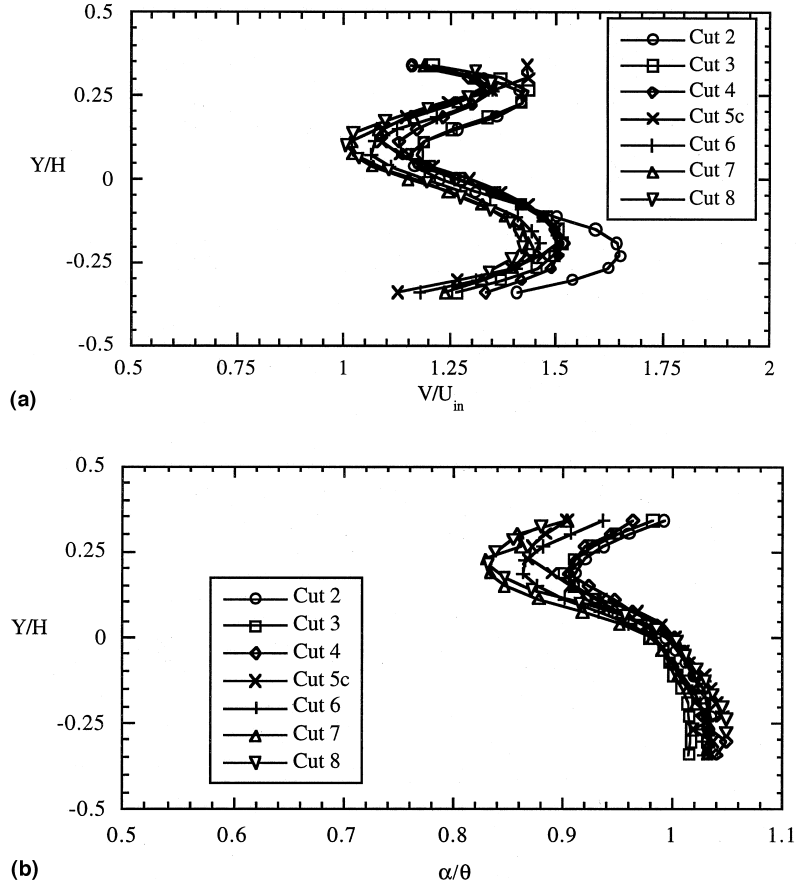

Fig. 8. Mean velocity measurements progressing streamwise through louver passages at Re = 230 showing: (a) normalized velocity magnitude; and (b) ratios of flow to louver angle.

passage at $Y/H = 0.1$, the velocity defect is still evident from the upstream louver wake. Note that geometrically the upstream louver occurs nearer to the top of the passage, as was illustrated in Fig. 4. The total velocity magnitude, normalized by the inlet velocity, are values greater than one due to the thick boundary layers present on the louvers themselves thereby causing a flow acceleration in the louver passages. In general, velocity magnitudes are slower near the top of the passage ($Y/H > 0$) than at the bottom of the passage.

The flow angles for each louver, shown in Fig. 8(b), indicate that near the top of the louver passage the flow angles fall below those occurring near the bottom of the passage. The louver blockage that decelerates the flow in the top of the passage causes a thicker boundary layer to develop on the downstream side of the louver as compared with the upstream side of the louver. As a result of this thicker boundary layer, the flow is being deflected away from the louver angle more at the top of the louver passage than at the bottom of the louver passage. Progressing downstream, the total velocity profiles indicate that the flow is decelerating slightly while the flow angles are continuing to decrease near the downstream side of the top louver ($Y/H > 0$) with very little change on the upstream side of the bottom louver.

Fig. 9(a) and (b) show a comparison of the total velocity profiles and flow angles at the middle position in the louver 5 passage for all three Reynolds numbers. Similar to the $Re = 230$ case, the total velocity profiles for the higher Reynolds numbers become similar beyond louver 2. In contrast with the $Re = 230$ case, the $Re = 1016$ case has total velocity magnitudes much closer to and even below one because of the thinner boundary layers that develop along the louvers. As the Reynolds numbers increase from $Re = 230$ to 1016, there is an increase in the velocity deficit from the upstream louver wake in the top portion of the louver passage. The largest difference, however, between these Reynolds numbers occurs near the bottom of the louver passage. While there is a high velocity occurring for the $Re = 230$ case at $Y/H = -0.2$, there is a flat region in the velocity occurring for the $Re = 450$, and a low velocity occurring for the $Re = 1016$ case. At $Re = 1016$, this low-speed fluid at $Y/H = -0.2$ in louver 5 occurs because of remnants from the large velocity deficit in louver 3 or, in general terms, from the large velocity deficit from two louver positions upstream.

The flow angles for the three Reynolds numbers, shown in Fig. 9(b), indicate that there is not as much variation throughout the louver passage at the high

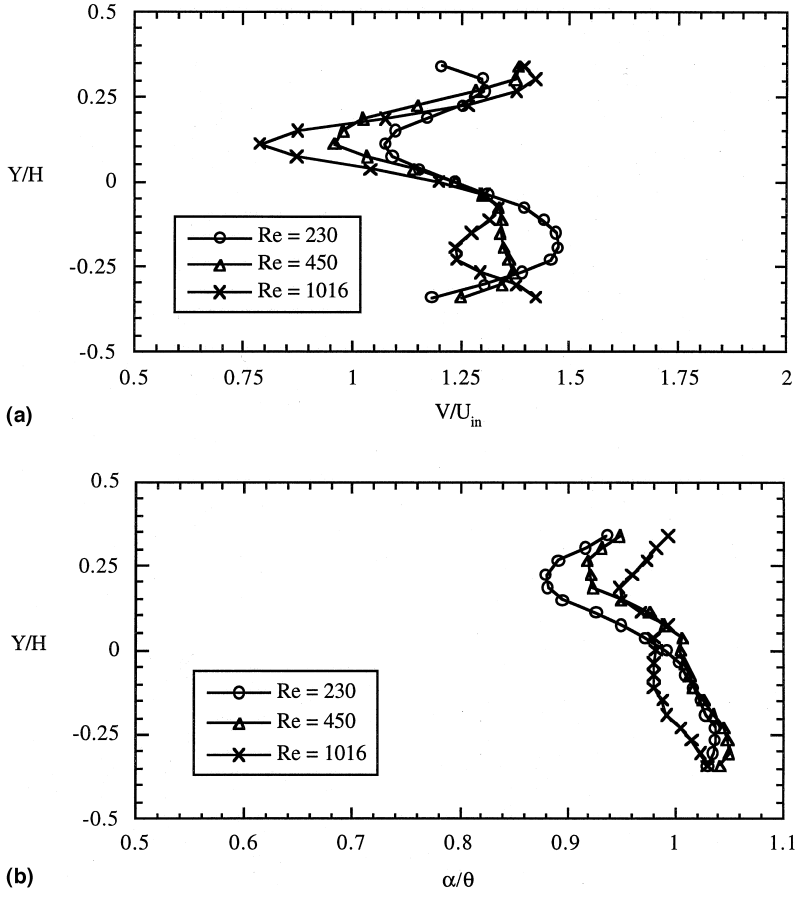

Fig. 9. Mean velocity measurements at cut 5c indicating Reynolds number effects on: (a) normalized velocity magnitude; and (b) ratio of flow angle to louver angle.

Reynolds number as compared with the low Reynolds number. This smaller variation can be attributed to the fact that the boundary layers that develop along the upstream and downstream sides of the louvers can be quite different where the downstream side of the louver has a thicker boundary layer than the upstream side. This effect was also reported by Zhang [11] who made predictions for a louvered fin at 25°. Zhang's results indicated for Re > 100, lower Nusselt numbers, averaged along the surface, occurred on the downstream side as compared with the upstream side of the louver. As the Reynolds numbers increased to Re $\geqslant$ 1000, the Nusselt numbers on the upstream and downstream side of the louvers were essentially the same.

Boundary layer measurements made along the louver indicated that near the leading edge of the louver, the boundary layer on the downstream side was approximately 20% thicker than on the upstream side for Re = 230. The boundary layer thicknesses for the Re = 1016 case indicated no difference between the upstream and downstream sides of the louver. In addition, the boundary layer thickness near the trailing edge of the louver was two times thicker for the Re = 230 case relative to the Re = 1016 case.

Fig. 10(a)–(c) show the measured velocity vectors as the flow progresses through louver 5 for the three Reynolds numbers. The strong deflection for Re = 230 on the downstream side of the top louver, as discussed previously, is quite evident from these vectors. The wake region downstream of the previous louver is evident at all three Reynolds numbers. The difference, however, is that while there is no indication of a wake region at the exit of the passage for Re = 230, the profiles do indicate a fairly strong wake region at the exit of the passage for Re = 1016 which then enters the next louver passage. It is also clear from these vectors that the wake from the previous set of louvers is still present for the Re = 1016 case entering the bottom side of the louver passage.

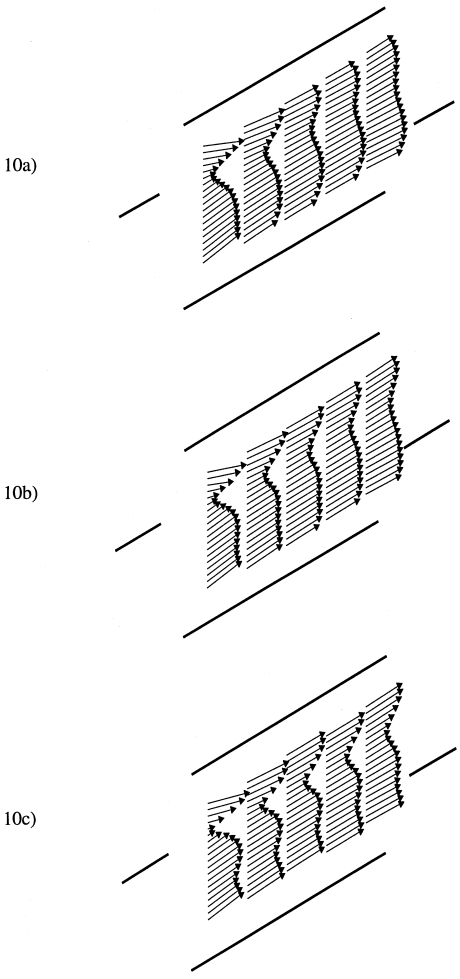

Fig. 10. Measured mean velocity vectors progressing through the fifth louver passage at: (a) Re = 230; (b) Re = 450; and (c) Re = 1016.

6. Time resolved flowfield results

Measurements to quantify the flow unsteadiness behind the louver, whether it be a flow instability or full vortex shedding, have not been presented in the open literature for louvered fins. Some studies, such as those reported by Amon et al. [12], Zhang et al. [8], and DeJong and Jacobi [7], have attempted to quantify frequencies from interrupted surfaces through simulations or flow visualization studies. To address the question as to when this unsteadiness occurs, we took the approach of calculating the energy spectral density of the measured velocity fluctuations for a range of Reynolds numbers behind the fifth streamwise louver. The velocity component used for these measurements was a component parallel to the louver direction at a position one-half of the louver length downstream of the louver. Spectra for the axial velocity and normal velocity components were also calculated and shown to agree in terms of the peak frequency with the velocity component parallel to the louver.

Care had to be taken in using this approach for two reasons. First, since the LDV gives measurements only when a particle passes through the probe volume, a method was devised such that the measured velocity data could be sampled at equally-spaced time intervals. Second, provisions were made to ensure that the inlet flow conditions did not have fan-induced dominant frequency, as discussed earlier, that would influence the shedding frequency.

Time resolved LDV velocity data were obtained by defining a timestep window, where that window was typically larger than most of the time between data points. All of the velocities taken during that timestep window were then averaged to obtain a velocity in the center of the timestep window. If no averages occurred in that timestep window, a linear interpolation between the two windows on either side was computed and used. Fig. 11 shows a small sample of the discrete velocity measurements for Re = 1000 and the equally spaced

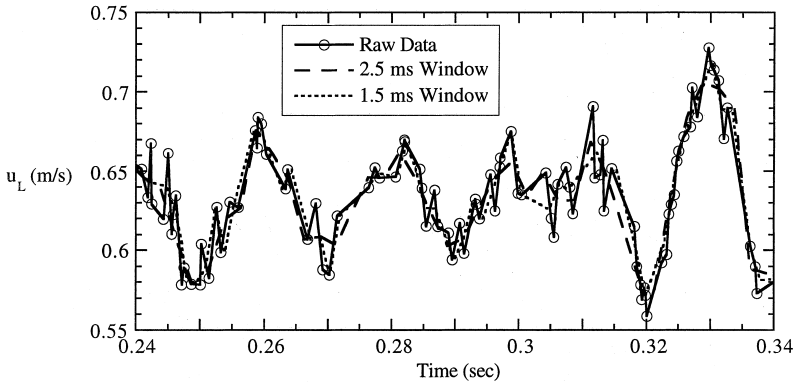

Fig. 11. Example of raw velocity measurements downstream of the fifth louver compared with equally-spaced velocities using two window sizes over a small time period at Re = 1000.

data that were put into the FFT program for two different window sizes of 1.5 and 2.5 ms. These instantaneous velocity measurements show a distinct periodicity to the flow with about a 50 Hz frequency. The equally spaced data, obtained using the procedure described, represents the flow periodicity quite well for both sample window sizes. The computed energy spectra using the two different window sizes agree quite well indicating an insensitivity to the window size.

The second requirement, a provision for a quiet flow at the inlet, was evaluated by calculating the spectra at the inlet, as discussed earlier. Spectra at the test section inlet were calculated for the entire range of Reynolds numbers to ensure that the flow was quiet for all conditions. Fig. 12 compares normalized spectra at the inlet for Re = 1000 with that occurring downstream of louver 5 at various Reynolds numbers. The normalized energy is plotted against a normalized frequency, or wave number. This inlet spectra is typical of what occurred at the test section inlet with no detected fan frequencies.

Fig. 12 clearly shows that there is a dominant frequency that occurs at Re = 1000. For Re $\leqslant$ 900, there was no dominant frequency. The spectra indicated that as the Reynolds number increases, the peak frequency shifted to higher and higher frequencies such that when using the local convection velocity these peaks collapsed to the same wave number, as indicated in Fig. 12. Subharmonics of the peak frequency, at twice the primary frequency, are also evident for Re $\geqslant$ 1100. The rms of the velocity fluctuations, relative to the local mean velocity, increased from 3.7% at Re = 1000 to 14.5% at Re = 1300 and remained at that level to Re = 1900. The Strouhal number (based on the fin thickness, peak frequency, and the local mean velocity) for each of these Reynolds numbers was calculated and found to be a constant at St = 0.171 ± 0.005 for 1000 < Re < 1900. This Strouhal number is similar to results for flow over inline and staggered parallel fins by Zhang et al. [11], which vary from 0.14 to 0.17 depending on the operating Reynolds number.

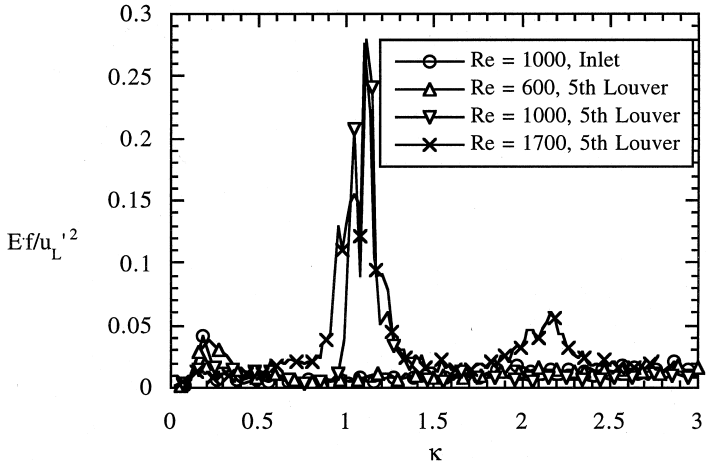

Fig. 12. Energy spectra versus wave number for measured velocity fluctuations at the inlet and downstream of the fifth louver for a range of Reynolds numbers.

7. Practical significance of these results

This paper has pointed out a number of practical issues associated with the experimental design of a louvered fin test section. With regards to the experimental design, the importance of using a tool such as CFD to design the experiment and ensure flow periodicity became evident. The CFD results from the louvered fin study with only five rows clearly showed that the wrong conclusions could be made as to whether the flow is duct or louver directed. The question of whether CFD can be used as a reliable design tool by insuring that CFD predictions using periodic boundary conditions can reproduce experimental measurements depends on a correct representative experimental design. Based on the experience of the authors in trying to quantify frequencies of the flow unsteadiness, care was needed to obtain a closed-loop flow system in which the inherent fan frequencies did not affect the measurements. The motor controlled fan with no in-line valve and with the Styrofoam packaging popcorn in the plenum did, in fact, allow a quiet flow to be achieved.

These results have also pointed out the importance of understanding the flowfield in order to enhance the heat transfer capabilities of louvered fins. The flowfield measurements clearly show that the flow was louver directed even at a Reynolds number of $Re = 230$ and became louver directed just after the first inlet louver. From that standpoint, this particular geometry would be very effective in terms of heat transfer. These results also indicated that near the leading edge of the louver the downstream side has a slightly thicker boundary layer than the upstream side at $Re = 230$, which would result in a higher heat transfer on the upstream side of the louver. At $Re = 1016$, it became apparent that the boundary layers are much closer to being the same thickness on the upstream and downstream sides of the louvers, which would result in the same heat transfer on both sides of the louver. In addition to the thinner boundary layers at $Re = 1016$ that would promote higher heat transfer, it is also expected that the unsteadiness of the flow leaving the louver and entering into the next downstream louver passage would promote heat transfer. These results indicate that from an optimizing standpoint, the operating range of the louvered fin heat exchanger needs to be considered. For example, at the higher Reynolds number, positioning the louver such that its vortex comes into contact with the downstream louver is important. Future work will entail documenting the flowfields for other geometries.

8. Conclusions

Optimizing the louvered fin geometry for compact heat exchangers is important for improving the heat transfer capabilities and reducing the space, weight, and cost requirements. To perform that optimization either through experimentation or computations, however, requires that the flowfields dictating both the heat transfer and pressure drop need to be understood. The results of this study have pointed out the importance of correctly designing an experimental facility to simulate the numerous rows of louvered fins occurring in a compact heat exchanger. The measured flowfields confirmed that, in fact, the flow is louver directed for this geometry at $230 \leqslant Re \leqslant 1016$.

Differences in the flowfield for $Re = 230$ as compared with $Re = 1016$ were detected both by the mean and time-resolved velocity measurements. For the $Re = 1016$ case the mean velocities indicated that wakes leaving the set of louvers located one and two louvers upstream were still evident while for the $Re = 230$ case the mean velocities indicated that only the wake from one louver upstream was evident. The velocity measurements indicated that the boundary layer on the downstream side of the louver was slightly thicker than on the upstream side of the louver. The time-resolved velocity measurements were analyzed in terms of spectra to obtain the peak frequency of the velocity fluctuations. The results indicated that for $Re \geqslant 1000$, there was a distinct frequency that occurred where the Strouhal number was constant at $St = 0.17$ in the range $1000 \leqslant Re \leqslant 1900$.

Nomenclature

E	energy spectra of velocity fluctuations
f	frequency
F_P	fin pitch
H	vertical distance between louvers, $H = F_p - t/\cos\theta$
l	louver length
L_P	louver pitch
Re	Reynolds number $= \rho U_{in} L_P/\mu$
St	Strouhal number, $St = ft/u_L$
t	fin thickness
u	mean streamwise velocity component
u_L	mean velocity component parallel to louver
u'_L	rms of velocity fluctuation parallel to louver
U_{in}	inlet face velocity
v	mean vertical velocity component
V	mean velocity magnitude $= (u^2 + v^2)^{1/2}$
X	streamwise coordinate direction
Y	vertical coordinate direction relative to louver, see Fig. 4
α	flow angle $= \tan^{-1}(v/u)$
$\overline{\alpha}$	averaged flow angle across louver passage
κ	wave number $= 2\pi ft/u_L$
μ	air viscosity
θ	louver angle
ρ	air density

Acknowledgements

The authors would like to acknowledge Modine Manufacturing Company for providing the scaled-up louver models and, in particular, Drs. Steve Memory, Mark Voss, Jonathan Wattelet, and Winston Zhang for serving as contract monitors for this work. The authors

would also like to thank Mr. David Cabrera for his contribution to this project.

References

[1] F.N. Beauvais, An aerodynamic look at automobile radiators, SAE Paper No. 650470, 1965.
[2] A. Achaichia, T.A. Cowell, Heat transfer and pressure drop characteristics of flat tube and louvered plate fin surfaces, Exp. Thermal Fluid Sci. 1 (1988) 147–157.
[3] C.J. Davenport, Heat transfer and fluid flow in louvered triangular ducts, Ph.D. Thesis, CNAA, Lanchester Polytechnic, 1980.
[4] R.L. Webb, P. Trauger, Flow structure in the louvered fin heat exchange geometry, Exp. Thermal Fluid Sci. 4 (1991) 205–217.
[5] K. Suga, H. Aoki, Numerical study on heat transfer and pressure drop in multilouvered fins, ASME/JSME Thermal Eng. Proc. 4 (1991) 361–368.
[6] A.A. Antoniou, M.R. Heikal, T.A. Cowell, Measurements of local velocity and turbulence levels in arrays of louvered plate fins, Heat Transfer, Paper No. 10-EH-18, 1990, pp. 105–110.
[7] N.C. DeJong, A.M. Jacobi, An experimental study of flow and heat transfer in parallel-plate arrays: local, row-by-row, and surface average behavior, Int. J. Heat Mass Transfer 40 (6) (1997) 1365–1378.
[8] L.W. Zhang, S. Balachandar, D.K. Tafti, F.M. Najjar, Heat transfer enhancement mechanisms in inline and staggered parallel-plate fin heat exchangers, Int. J. Heat Mass Transfer 40 (10) (1997) 2307–2325.
[9] FLUENT/UNS, User's Guide, Release 4.0, Fluent, Inc., Lebanon New Hampshire, 1996.
[10] R.J. Moffat, Describing the uncertainties in experimental results, Exp. Thermal Fluid Sci. 1 (1988) 3–17.
[11] L.W. Zhang, A numerical study of flow and heat transfer in compact heat exchangers, Ph.D. Dissertation, University of Illinois, Urbana, Illinois, 1996.
[12] C.H. Amon, D. Majumdar, C.V. Herman, B.B. Mikic, Fast-evolving transport phenomena in self-sustained communicating-channels flows, presented at the 1993 ASME Winter Annual Meeting, New Orleans, Louisiana, Experimental and Numerical Flow Visualization, FED-vol. 172, 1993, pp. 351–358.